A CLAS Collaboration Proposal to PAC47

Search for a $\phi - N$ Bound State from ϕ Production in a Nuclear Medium

Haiyan Gao[†‡], Chao Gu, Vladimir Khachatryan, Xiaqing Li, Tianbo Liu[†], Andrew Smith, Weizhi Xiong, Zhiwen Zhao[†], Jingyi Zhou, Anselm Vossen

Duke University, Durham, NC 27708, USA

Whitney R. Armstrong, Kawtar Hafidi, Zein-Eddine Meziani

Argonne National Laboratory, Lemont, IL 60439, USA

Gabriel Charles, Raphael Dupré

Institut de Physique Nucléaire, CNRS-IN2P3, Université Paris-Sud, Université Paris-Saclay, 91406 Orsay Cedex, France

James A. Dunne, Dipangkar Dutta, Lamiaa El Fassi

Mississippi State University, Miss State, MS 39762, USA

Hongxia Huang

Nanjing Normal University, Nanjing, Jiangsu 210097, China

Ashot Gasparian

North Carolina A&T State University, Greensboro, NC 27411, USA

Mohammad Hattawy

Old Dominion University, Norfolk, VA 23529, USA

Nathan Baltzell[†], Eugene Pasyuk

Thomas Jefferson National Accelerator Facility, Newport News, VA 23606, USA

Jixie Zhang

University of Virginia, Charlottesville, VA 22904, USA

and the CLAS Collaboration

[†]Spokesperson

[‡]Contact person: gao@phy.duke.edu

Abstract

In light of recent experimental results of the hidden charm pentaquark candidates at LHCb, a renewed interest is invoked for other multi-quark states also. The QCD van de Waals interaction, mediated by multi-gluon exchanges, is expected to dominate the interaction between two hadrons when they have no common quarks, which led to the prediction that a bound state between a J/ψ and a light nucleus can exist. It has also been suggested by theoretical studies that a ϕ-meson and a nucleon may form a bound state. Studies also suggest that such a bound state can be produced via two steps: first the production of a ϕ-meson from a nucleon near the threshold or below the threshold in a nuclear target, and then the ϕ-meson interacts with another nucleon inside the nucleus to form the bound state. Since the $\phi - N$ bound state can be viewed as a hidden strange pentaquark state, a comparison with the hidden charm pentaquark candidates could help unveil the flavor dependent effect in hadron physics.

We propose to perform a measurement of quasi-real photo-production from a nuclear target to search for a $\phi - N$ bound state with a predicted mass value near 1950 MeV and a total decay width of 4 MeV. Because the probability of the formation of the bound state is enhanced at a low relative velocity between the ϕ-meson and the nucleon, we propose to search for this bound state through the sub- and near-threshold ϕ-production on a gold target in Hall B at JLab. The scattered electrons would be detected by the forward tagger, and the proton, K^+, and K^- in the final state would be detected by the ALERT detector and the CLAS12 forward detector to reconstruct the bound state. The total beam time requested is 45 days for this experiment. The proposed experiment will be a pioneer to explore the strange multi-quark final states in the JLab 12 GeV era and lead a new way of studying hadron physics and non-perturbative QCD through searches of exotic QCD states.

Contents

1 Introduction

The multi-quark state is one of the active frontiers since the establishment of the quark model [1]. Hadrons, as color singlet states, are composite particles made of quarks and gluons held together by strong interactions. Ordinary mesons are described as quark-antiquark states and ordinary baryons are described as three-quark states. Exotic mesons, such as glueballs, tetraquarks, and hybrid mesons, have quantum numbers that are impossible for a quark-antiquark configuration. Similarly, exotic baryons have constituents other than the three-quark configuration. The pentaquark is a kind of exotic baryons whose minimum-quark-content is five-quark. The quantum chromodynamics (QCD) is currently known as the fundamental theory of strong interactions in the framework of the Yang-Mills gauge theory with quarks and gluons as degrees of freedom. It allows the existence of multi-quark states. Due to the non-perturbative nature of QCD at low energy scales, first principle calculation of all hadronic properties is still a challenging issue. Hence experimental study of multi-quark states is an important approach to understand the dynamics of the strong interaction at the hadronic scale.

In 2015, LHCb discovered two hidden charm pentaquark candidates, names as $P_c(4380)$ and $P_c(4450)$, in the channel $\Lambda_b \to J/\psi K^- p$ [2], which contains narrow peaks in the $J/\psi p$ invariant mass distribution. In 2019, LHCb followed up with an order of magnitude more data to discover another narrow pentaquark candidate $P_c(4312)^+$ and to confirm that $P_c(4450)^+$ consists of two narrow overlapping peaks, $P_c(4440)^+$ and $P_c(4457)^+$ [3]. This discovery invoked a renewed interest in this field [4]. As the strangeness counterpart, whether hidden strange pentaquark states exist or not becomes an interesting issue, and some theoretical explorations have been performed [5–8]. However, the extension of heavy pentaquarks that have at least one charm or bottom quark, to light pentaquarks that have no heavy quark constituents is nontrivial. Up to now, almost all discovered multi-quark states or candidates contain at least one heavy quark constituent. Therefore, experimental search for light pentaquarks, *e.g.* hidden strange pentaquarks, is of particular interest and of unique significance to understand the flavor-dependent properties of multi-quark states.

In this experiment, we propose to search for a hidden strange pentaquark state: the $\phi - N$ bound state. The interaction between two hadrons is usually mediated by meson exchange. However, Brodsky, Schmidt, and de Téramond point out that the QCD van de Waals force, mediated by multi-gluon exchange, will become the dominant interaction between two hadrons when they have no common quarks [9], and they predict that such attractive force is strong enough to bind a charmonium to a nucleus. Luke, Manohar, and Savage further show that the QCD van de Waals force is enhanced at low relative velocities between the two hadrons [10]. It supports the prediction that a nucleon/nucleus-charmonium bound state can be produced near the charm production threshold. As an extension to the strangeness, one expects the ϕ meson, which is almost a pure $s\bar{s}$ state, could also be bound to a nucleon/nucleus. A lattice QCD simulation [11] has been performed for both the charmonium and the strangeonium cases showing that the interaction between the

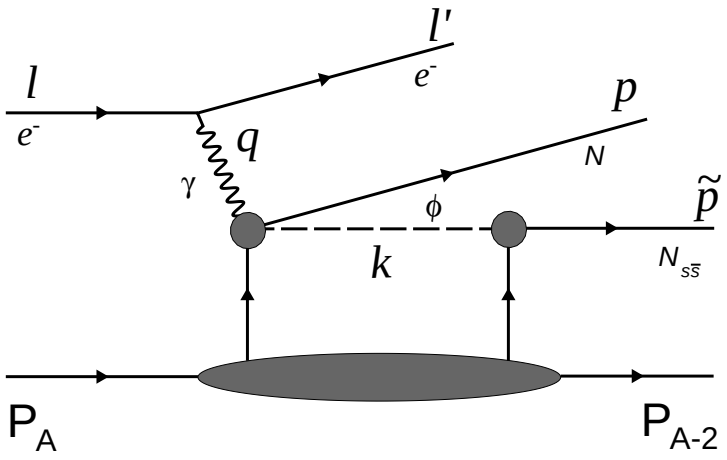

Figure 1: The mechanism of the $\phi - N$ bound state production on a nuclear target. This figure is from Ref. [14].

charmonium/strangeonium and the nucleon/nucleus could be strong enough to form a bound state.

The $\phi - N$ bound state was first explored by Gao, Lee, and Marinov [12] with a Yukawa type attractive potential between the ϕ and the nucleon to mimic QCD van de Waals interactions. It is also shown that the sub-threshold quasi-free ϕ meson production inside a nuclear medium will enhance the probability for the formation of the $\phi - N$ bound state. A mechanism to produce such $\phi - N$ bound state is illustrated in Figure 1. In this illustration, the reaction takes place in two steps. First the ϕ meson is produced from a nucleon in a nuclear medium, and then it interacts with another nucleon inside the nucleus to form the bound state. The subthreshold production of ϕ-mesons from a nuclear target has been established in experiment [13] using a deuterium target, and it was pointed out that heavier nuclear targets would be ideal for future dedicated searches for a $\phi - N$ bound state.

Later on, a more careful model calculation was carried out by Huang, Zhang, and Yu [15]. Including the channel coupling effect, the $\phi - N$ bound state with a few MeV binding energy was found in the extended chiral quark model calculation. Recently, a study of the hidden strange light baryon-meson system was performed in the quark delocalization color screen model [14]. A $\phi - N$ bound state around 1950 MeV with about 4 MeV decay width was found. This finding is consistent with the predictions in previous studies. A simple Monte Carlo simulation showed the feasibility to search for the $\phi - N$ bound state at Jefferson Lab. The existence of such a $\phi - N$ bound state is further confirmed in the Bethe-Salpeter equation calculation [16]. Therefore, the existence of such $\phi - N$ bound state is favored by various model calculations, and an experimental search will help clarify this interesting issue, i.e. whether such a bound state exists or not.

Following the study in Refs. [12, 14, 17], we propose to search for the $\phi - N$ bound state through the quasi-real photo-production on a nuclear target near the threshold of the ϕ meson production as such kinematics enhance the interaction between the produced ϕ meson and nucleons inside the nucleus. Based on the theoretical study of the decay properties of this bound state, the decay of the bound state is dominated by the decay of the bound ϕ meson. Thus it can be experimentally reconstructed via the pK^+K^- channel.

Apart from the $\phi-N$ bound state, the ϕ meson production in a nuclear medium is also an interesting issue. The changes of light meson properties in a nuclear medium have attracted much interest in nuclear physics [18], and among them there is special significance on the ϕ meson. Despite ϕ meson is almost a pure $s\bar{s}$ state, it strongly interacts with a nucleus, which is dominantly composed of u and d quarks, via multi-gluon exchanges or below-threshold virtual kaon-antikaon exchanges. The possible in-medium mass shift of ϕ meson is strongly correlated to the strangeness content of the nucleon, which is proportional to the strange σ-term of the nucleon [19]. The determination of the strange σ-term is important for understanding the proton mass budget [20, 21]. It also has implications beyond strong interactions, *e.g.* the experimental search for dark matter [22–24]. A possible downward shift of the ϕ meson mass in a nuclear medium has been theoretically suggested for a long time [25, 26]. Experimentally, a 3.5% ϕ meson mass reduction was reported by the KEK-PS E325 Collaboration using a copper target [27]. Such a few percent downward mass shift is favored in a recent theoretical calculation [28]. In addition, a broaden width of the ϕ meson in a nuclear medium is measured in several experiments [27, 29–31], but the values differ in a wide range. Therefore, this proposed experiment may also help measure the in-medium modifications of ϕ meson properties. Besides, the produced ϕ meson can also be bounded to nuclei [11, 32, 33].

On the other hand, measurements of the electro-production of ϕ meson near the threshold can help us understand the enhancement of differential cross section of ϕ meson photo-production around $W = 2.1$ GeV [34–36]. Some resonances around such a mass value are suggested in theoretical studies [37–39] to explain the experimental result. Hence, the measurement in this proposed experiment will also help clarify this issue.

The proposal is organized as follows. We first briefly review theoretical predictions of the $\phi - N$ bound state in Section 2, and then we describe the experiment setup for this measurement in Section 3.1. Simulations, projections, beam time request and trigger are discussed in Section 4. A summary is drawn in the last section.

2 Theoretical Predictions

Although the $\phi - N$ bound state has not been observed in experiment, theoretical studies using various approaches support the existence of such a bound state. The experiment proposed here aims at establishing whether the $\phi - N$ bound state exists or not. One will focus on understanding the mechanism of the formation of the bound state once it is discovered. In this section, we briefly review several theoretical calculations which predict the existence of the $\phi - N$ bound state.

2.1 Chiral Quark Model

The nonperturbative effect of the underlying theory, QCD, is important for light quark systems, but it is difficult to have first principle solutions. QCD-inspired phenomenlogical models are needed to calculate experimental observables. The chiral quark model is proven successful in reproducing the energies of the baryon ground states, the binding energy of the deuteron, the nucleon-nucleon scattering phase shifts, the hyperon-nucleon scattering cross sections, and baryon-meson scattering processes [40].

The $\phi - N$ system is dynamically studied in the chiral quark model and the extended quark model in Ref. [15]. In the model, hadrons are described with quarks as the degrees of freedom and gluons are sublimated to the potential between quarks. The Hamiltonian of the light baryon-meson system, which contains four quarks and one antiquark, is expressed as

$$H = \sum_{i=1}^{5} T_i - T_{\text{c.m.}} + \sum_{i<j=1}^{4} V_{ij} + \sum_{i=1}^{4} V_{i\bar{5}}, \tag{1}$$

where T_i is the kinetic energy of the i-th constituent, $T_{\text{c.m.}}$ is the kinetic energy of the center-of-mass motion, V_{ij} is the quark-quark interaction, and $V_{i\bar{5}}$ is the quark-antiquark interaction.

The quark-quark interaction can be expressed into several terms according to their physical origins as

$$V_{ij} = V_{ij}^{\text{OGE}} + V_{ij}^{\text{conf}} + V_{ij}^{\text{chiral}}, \tag{2}$$

where V_{ij}^{OGE} is the one-gluon-exchange potential, which is obtained from the leading order calculation of the quark-quark scattering amplitude, V_{ij}^{conf} is the confinement potential, which dominates the long distance interaction, and V_{ij}^{chiral} is the chiral fields induced quark-quark potential. In the chiral SU(3) quark model, V_{ij}^{chiral} includes scalar meson (σ) exchanges and pseudo-scalar meson (π) exchanges. In the extended chiral SU(3) quark model, vector meson (ρ) exchanges are also included.

The quark-antiquark protential $V_{i\bar{5}}$ term includes two parts:

$$V_{i\bar{5}} = V_{i\bar{5}}^{\rm ann} + V_{i\bar{5}}^{\rm dir}. \tag{3}$$

The annihilation term $V_{i\bar{5}}^{\rm ann}$ is obtained via the subprocess that the quark and the antiquark annihilates into a gluonand, and the direct interaction term $V_{i\bar{5}}^{\rm dir}$ is similar to the quark-quark interaction,

$$V_{i\bar{5}}^{\rm dir} = V_{i\bar{5}}^{\rm OGE} + V_{i\bar{5}}^{\rm conf} + V_{i\bar{5}}^{\rm chiral}, \tag{4}$$

where

$$V_{i\bar{5}}^{\rm chiral} = \sum_j (-1)^{G_j} V_{i\bar{5}}^{{\rm chiral},j}, \tag{5}$$

where G_j is the G-parity of the j-th meson.

Model parameters are taken from previous studies [41, 42] on baryon ground states, deuteron binding energy, and NN scattering phase shifts. The $\phi - N$ system is then dynamically solved with the resonating group method, which is a well established method for studying the interaction between two composite particles. In the calculation, the channel coupling effect to ΛK^*, which contains the same quark content as the $N\phi$ system, is included. The tensor force, which means a mixing between the S-wave and the D-wave, is also taken into account, but the effect is tiny for the $N\phi$ system and can be neglected. The attractive interaction between ϕ and N is dominated by the σ exchange together with the channel coupling effect. The calculation in the extended chiral quark model finds that the attraction is strong enough to form a $\phi - N$ bound state with several MeV binding energy.

2.2 Quark Delocalization Color Screening Model

The quark delocalization color screening model is developed aiming to understand the similarities between nuclear and molecular forces despite different scales. The intermediate-range attraction is achieved by the quark delocalization, which is like the electron percolation in molecules. The color screening provides an effective description of the hidden color channel coupling [43], and leads to the possibility of the quark delocalization. This model was utilized to investigate the baryon-baryon scattering phase shifts. It provides a good description of the nucleon-nucleon and nucleon-hyperon interactions and the deuteron properties [44–47]. Some dibaryon candidates are also studied with this model [48, 49]. The one of particular interest is a narrow resonance $N - \Omega$ state [50], which is proposed for searches in heavy ion collisions and a hadron beam experiment with a newly developed automatic scanning system. Moreover the hidden charm pendaquark candidates, $\eta_c - N$ and $J/\psi - N$ bound states, are also studied in this model [51].

The light baryon-meson system with hidden strange is studies in the quark delocalization color screening model in Ref. [14]. In this model, the Hamiltonian of the baryon-meson system is expressed as

$$H = \sum_{i=1}^{5}\left(m_i + \frac{\boldsymbol{p}_i^2}{2m_i}\right) - T_c + \sum_{i<j}\left[V^G(r_{ij}) + V^\chi(r_{ij}) + V^C(r_{ij})\right], \tag{6}$$

where

$$V^G(r_{ij}) = \frac{1}{4}\alpha_s \boldsymbol{\lambda}_i\cdot\boldsymbol{\lambda}_j\left[\frac{1}{r_{ij}} - \frac{\pi}{2}\left(\frac{1}{m_i^2}+\frac{1}{m_j^2}+\frac{4\boldsymbol{\sigma}_i\cdot\boldsymbol{\sigma}_j}{3m_im_j}\right)\delta(r_{ij}) - \frac{3}{4m_im_jr_{ij}^3}S_{ij}\right] \tag{7}$$

is the gluon exchange potential,

$$\begin{aligned} V^\chi(r_{ij}) = \frac{1}{3}\alpha_{\rm ch}\frac{\Lambda_\chi^2}{\Lambda_\chi^2 - m_\chi^2}m_\chi \Bigg\{ &\left[Y(m_\chi r_{ij}) - \frac{\Lambda_\chi^3}{m_\chi^3}Y(\Lambda_\chi r_{ij})\right]\boldsymbol{\sigma}_i\cdot\boldsymbol{\sigma}_j \\ &+ \left[H(m_\chi r_{ij}) - \frac{\Lambda_\chi^3}{m_\chi^3}H(\Lambda_\chi r_{ij})\right]S_{ij}\Bigg\}\boldsymbol{\tau}_i\cdot\boldsymbol{\tau}_j, \quad \chi = \pi, K, \eta \end{aligned} \tag{8}$$

is the chiral field exchange potential, and

$$V^C(r_{ij}) = -a_c\boldsymbol{\lambda}_i\cdot\boldsymbol{\lambda}_j[f(r_{ij}) + V_0], \tag{9}$$

$$f(r_{ij}) = \begin{cases} r_{ij}^2 & \text{if } i,j \text{ occur in the same baryon orbit} \\ \frac{1-e^{-\mu_{ij}r_{ij}^2}}{\mu_{ij}} & \text{if } i,j \text{ occur in different baryon orbits} \end{cases}$$

is the effective confinement potential.

Here, the S_{ij} is the quark tensor operator:

$$S_{ij} = \frac{(\boldsymbol{\sigma}_i\cdot\boldsymbol{r}_{ij})(\boldsymbol{\sigma}_j\cdot\boldsymbol{r}_{ij})}{r_{ij}^2} - \frac{1}{3}\boldsymbol{\sigma}_i\cdot\boldsymbol{\sigma}_j. \tag{10}$$

The $\boldsymbol{\sigma}$ and the $\boldsymbol{\tau}$ are Pauli matrices that, respectively, describe the spin and the isospin spaces, and the $\boldsymbol{\lambda}$s are the Gell-Mann matrices that describe the color degrees of freedom. The $Y(x)$ and $H(x)$ are the standard Yukawa functions [52], the T_c is the center-of-mass kinetic energy, the $\alpha_{\rm ch}$ is the chiral coupling constant determined from the πN scatterings, the Λ_χ is the chiral symmetry breaking scale, and the α_s is the strong coupling constant. The μ_{ij} in the confinement potential V^C is determined from the deuteron properties, NN scattering phase shifts, and $N\Lambda$ and $N\Sigma$ scattering cross sections.

The quark delocalization effect is realized by specifying the single-particle orbital wave function as a linear combination of left and right Gaussians. It effectively results in an attractive interaction between the ϕ meson and the nucleon. With model parameters taken from previous studies, the hidden strange light baryon-meson system is solved in the framework of the resonating group method. Including the channel coupling effect, a $\phi - N$ bound state with several MeV binding energy is obtained in the quark delocalization color screening model. Furthermore the decay width of the bound state is calculated from the phase shifts in the resonance scattering processes, and about 4 MeV width is obtained.

2.3 Bethe-Salpeter Equation

The Bethe-Salpeter equation is a relativistic covariant approach to study two-body bound states in quantum field theories. The hidden strange $\phi - N$ system is studied in the Bethe-Salpeter equation approach in Ref. [16]. In this study, the multi-gluon mediated van de Waals force is described by a Yukawa type potential,

$$iV_{N\phi} = (4\pi)^2 \frac{\alpha}{q^2 - \mu^2} \bar{N} N \phi \cdot \phi, \tag{11}$$

where N is the spinor of the nucleon and ϕ is the polarization vector of the ϕ meson.

The effective Lagrangians that describe the coupling to the $\Sigma^* K$ channel are expressed as

$$\mathcal{L}_{KK\phi} = -ig_{KK\phi}[K^\dagger \phi^\mu \partial_\mu K + \partial_\mu K^\dagger \phi^{\mu\dagger} K], \tag{12}$$

$$\mathcal{L}_{K^*K\phi} = g_{K^*K\phi} \epsilon^{\mu\nu\sigma\tau} \partial^\mu K^{*\nu\dagger} \phi^\tau \partial_\sigma K, \tag{13}$$

$$\mathcal{L}_{K\Sigma^*N} = \frac{f_{K\Sigma^*N}}{m_K} \bar{N} \Sigma^{*\mu} \partial^\mu K + \text{H.c.}, \tag{14}$$

$$\mathcal{L}_{K^*\Sigma^*N} = i\frac{f_{K\Sigma^*N}}{m_K} \bar{N} \gamma_5 \gamma^\nu \Sigma^{*\mu} K^{*\mu\nu} + \text{H.c.}, \tag{15}$$

where the K, ϕ, K^*, N, and Σ^* are respectively the fields for K meson, ϕ meson, K^* meson, nucleon, and Σ^* baryon, the tensor $K^{*\mu\nu} = \partial^\mu K^{*\nu} - \partial^\nu K^{*\mu}$, and f/g are coupling constants.

Similarly, the effective Lagrangians that describe the coupling to the ΣK^* channel are expressed as

$$\mathcal{L}_{K^*K^*\phi} = i\frac{g_{K^*K^*\phi}}{2}(K^{*\mu\dagger}\phi_{\mu\nu}K^{*\nu} + K^{*\mu\nu\dagger}\phi_\mu K^{*\nu} + K^{*\mu\dagger}\phi_\nu K^{*\nu\mu}), \tag{16}$$

$$\mathcal{L}_{K^*K\phi} = g_{K^*K\phi} \epsilon^{\mu\nu\sigma\tau} \partial^\mu K^{*\nu\dagger} \phi^\tau \partial_\sigma K, \tag{17}$$

$$\mathcal{L}_{\Sigma KN} = \frac{g_{KN\Sigma}}{m_N + m_\Sigma} \bar{N} \gamma^\mu \gamma_5 \Sigma \partial_\mu K + \text{H.c.}, \tag{18}$$

$$\mathcal{L}_{\Sigma K^*N} = -g_{\Sigma K^*N} \bar{N} [\gamma^\nu - \frac{\kappa_{\Sigma\Sigma\rho}}{2m_\Sigma} \sigma^{\nu\rho} \partial_\rho] K^{*\nu} \Sigma + \text{H.c.}. \tag{19}$$

Together with the $\Sigma^* K$ and ΣK^* interactions obtained in previous studies [6, 53], one can solve the rescattering amplitude by inserting the interaction into the Bethe-Salpeter equation. To reduce the complexity of solving the Bethe-Salpeter equation in Minkowski space, a spectator quasi-potential approximation is introduced by putting baryons on shell. Then possible bound states produced from the $\Sigma^* K \to N\phi \to \Sigma K^*$ interaction is reflected by pole structures of the scattering amplitude. The result of the calculation in Ref. [16] shows that a $\phi - N$ bound state can be formed from the direct $N\phi$ interaction, which the channel coupling effect is small.

2.4 Summary

The $\phi - N$ bound state is suggested by various theoretical calculations, and the formation of this bound state is proposed to be dominated by different mechanisms: the σ exchange and the channel coupling effect in the chiral quark model, the quark delocalization effect in the quark delocalization color screening model, and the direct $N\phi$ interaction in the quasi-potential Bethe-Salpeter approach. An experimental search for the $\phi - N$ bound state will be very helpful concerning whether such a bound state exists or not in nature, which is the focus of the proposed experiment. Only after the discovery of such a bound state is made, then one should focus on understanding the underlying mechanism for its existence.

3 Experimental Setup

3.1 Overview

The proposed $\phi - N$ bound state search is based on theoretical studies supporting the existence of such a bound state with a favorable two-step production process for such a state from a heavy nuclear target. The first step is to produce a ϕ on a proton or neutron inside a nuclei. So it favors a target with large A. The second step is to let the ϕ interact with a nearby proton or neutron to form the bound state before decaying into NpK^+K^-. To limit our study to the detection of charged particles only, we consider the second step with a nearby proton only. This makes a target nuclei with large Z desirable. Gold (A=197 and Z=79) is a good nuclei target for this search and the factor that it can be made as thin foil also helps reduce potential energy loss of final state particles.

We carried out a study of the formation of a $\phi - N$ bound state through quasi-real photoproduction on a gold target. Such a study will provide some guidance about how to set up detectors to search for such a bound state.

The signal channel as illustrated in Figure 1, $e\text{Au} \to e'N[p\phi]X \to e'NpK^+K^-X$, is generated according to the model calculation in Section 2.2 and Ref. [14]. Its crosssection are shown in Figure 2 and virtual photon flux for the quasi-real photoproduction is added on top of it.

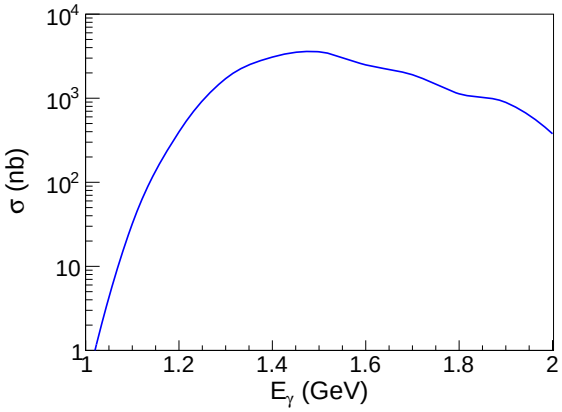

Figure 2: (color online) The cross section of the $N_{s\bar{s}}$ bound state photoproduction on a gold target. The cross section of $N_{s\bar{s}}$ photoproduction has a maximum below the threshold $E_\gamma = 1.57\,\text{GeV}$. This feature is consistent with the calculation in [12]. As expected, the cross section drops with the photon energy above the threshold because of the increasing ϕN relative momentum.

In addition to the channel of interest, four background channels with pK^+K^- in the final state are also generated. The first one is from the same reaction as the signal channel,

but the detected proton is not from the bound state decay. The second one is the ϕ-meson production process without the formation of the bound state. The amplitude extracted from the data in [35] is used to generate events in this channel. The third one is $\Lambda(1520)K^+$ production with $\Lambda(1520)$ decaying into pK^-. In this process, K^+ and K^- in the final state have different distributions. The near threshold production amplitude extracted from the data in [54] is used to generate events in this channel. The fourth one is the direct K^+K^- production near the threshold. We model this channel by using the amplitude of ϕ production but replacing the mass with the invariant mass of the K^+K^- system. During the event generation, the masses of ϕ and $\Lambda(1520)$ are sampled according to the Breit-Wigner distribution. The particles from decays are generated according to the phase space distribution in the center-of-mass frame and then boosted to the laboratory frame according to the momentum of the parent particle. The energy and momentum of the nucleon inside the gold nucleus is sampled according to the measurement of JLab E91-013 [55].

Taking into consideration both the requirement for the beam energy to be near the ϕ meson production threshold and the beam energy settings of the CEBAF accelerator, the beam energy of 4.4 GeV is found optimal [14]. In this study with event generators, we only assume that the beam energy is set at 4.4 GeV and the scattered electron is restricted between 2.5° and 4.5° in polar angle and between 1 GeV and 4 GeV in energy, which is within the CLAS12 forward tagger detection range. The final pK^+K^- from both signal and background channels are in their full phase space, not limited by any other detector acceptance, resolution, efficiency or any kinematic cut. In Figure 3, we show the invariant mass spectra of pK^+K^-, pK^+, pK^-, and K^+K^- from each channel. Those background channels are large in the full phase and we need to choose the right phase space to optimize signal detection.

The momentum-polar angle distributions of the generated proton and kaons from the bound state are shown in Figure 4. In Figure 5, we also show the momentum distributions of the proton and the kaon in the final state from each channel. One can observe that the proton and the kaons which are decay products from the bound state concentrate in the low momentum region separated from the other channels. It is clear that we need to detect pK^+K^- below 500 MeV and down to 100 MeV or lower to optimize the signal detection and we can cut away high energy particles to suppress the background.

From the study, we conclude that combining the forward tagger, CLAS12 main detector and a low energy recoil detector is the key for the success of this proposed experiment. After compare a few existing or already approved recoil detectors, the Low Energy Recoil Tracker (ALERT) detector which consists of a stereo drift chamber for track reconstruction and an array of scintillators for particle identification appears to be the best choice for our proposed experiment. This chapter will begin with a description of the CLAS12, the forward tagger and the ALERT detector. Some other options of the low energy recoil detectors like CLAS12 central detector and BONUS12, which are optimal for this proposal, are also mentioned in the appendix.

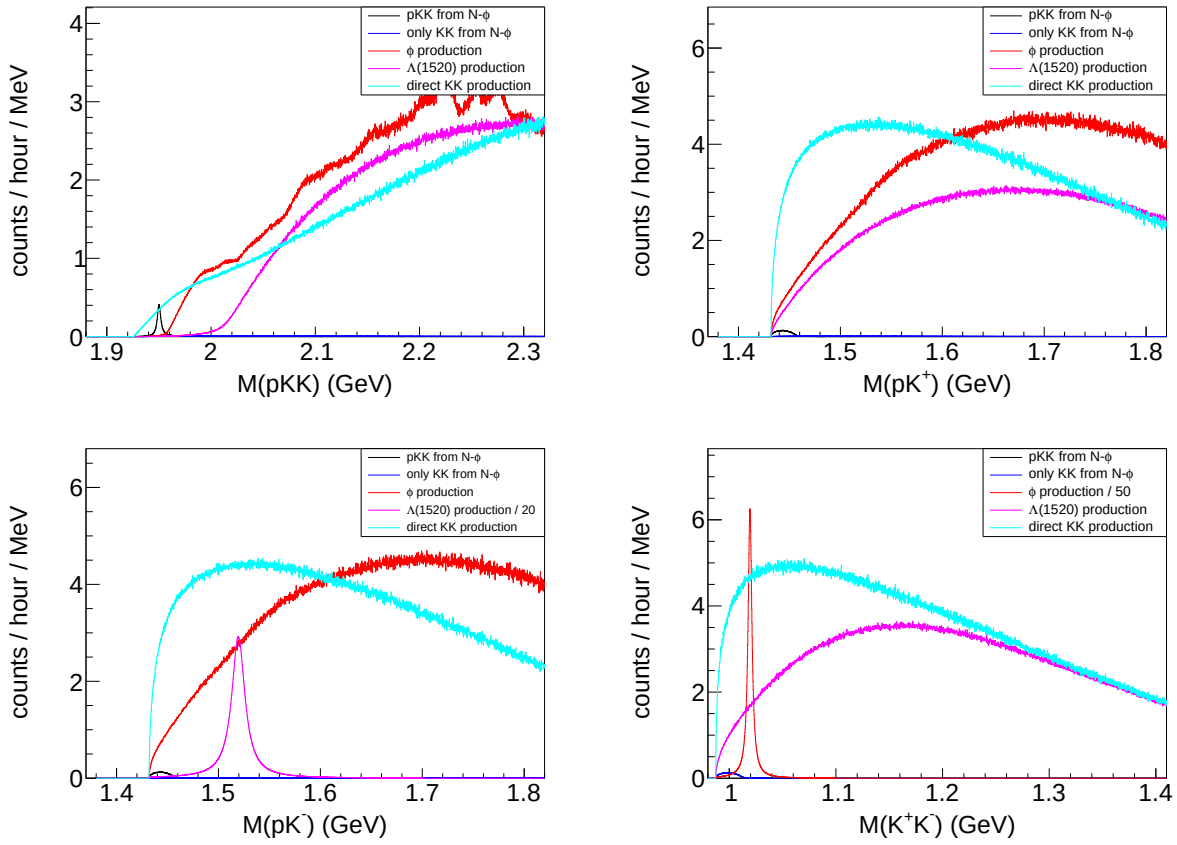

Figure 3: The invariant mass spectra of pK^+K^- (upper left), pK^+ (upper right), pK^- (lower left), and K^+K^- (lower right) from different channels. The black curves show the channel with pK^+K^- from the bound state decay, which is the signal channel. The blue ones show the channel with only K^+ and K^- from the bound state decay and the other proton in the bound state production. The red ones show the channel with ϕ meson production, the magenta ones show the channel with $\Lambda(1520)$ production, and the light blue ones show the channel with direct K^+K^- production. The pK^- spectrum of $\Lambda(1520)$ production channel is scaled by an additional factor of 1/20, and the K^+K^- spectrum of the ϕ production channel is scaled by an additional factor of 1/50 for visibility. All spectra in these plots are produced with electron beam energy 4.4 GeV on a 0.01 mm gold foil target, scattered electrons between 2.5 deg and 4.5 deg and between 1 GeV and 4 GeV and 3e34cm^{-2}s^{-1}luminosity.

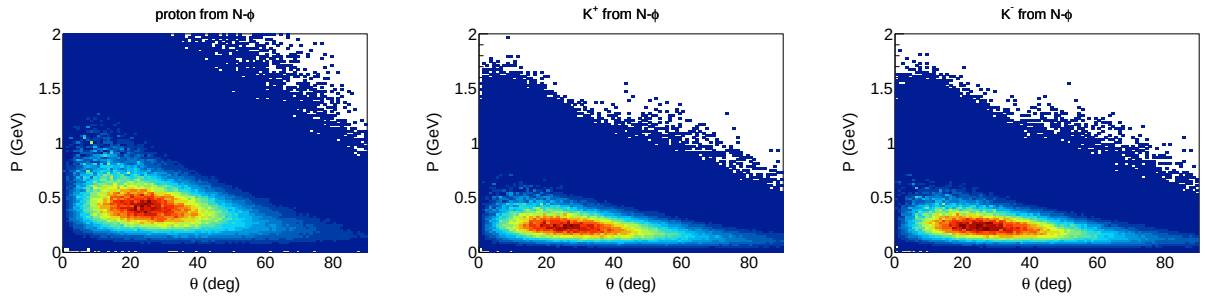

Figure 4: The momentum-polar angle distributions of the detected proton and kaons from the bound state. The left panel is the distribution of the detected proton, the middle panel is the distribution of the detected K^+, and the right panel is the distribution of the detected K^-. All spectra in these plots are produced with electron beam energy 4.4 GeV on a 0.01 mm gold foil target, scattered electrons between 2.5 deg and 4.5 deg and between 1 GeV and 4 GeV and 3e34cm^{-2}s^{-1}luminosity.

It is important to bear in mind that while the proposed search is based on theoretical studies supporting the existence of such a bound state and a favorable two-step production process for such a state from a heavy nuclear target, the search itself does not depend on the detailed production mechanism. Rather it depends on the decay of such a bound state and how well the kinematic distribution of the decay particles from the bound state can be distinguished from other channels that share the same final state particles.

3.2 CLAS12 and Forward Tagger

The CLAS12 detector in Hall B is designed to carry out experiments using high energy electron beams incident on polarized and unpolarized targets at luminosities up to $L = 10^{35}$ cm^{-2} sec^{-1}. CLAS12 consists of two parts, the forward detector (FD) and the central detector (CD) [56]. The design characteristics of CLAS12 and Forward tagger are presented in Table 1.

The forward detector is able to detect and identify charged and neutral particles scattered between 5° and 35° over the full momentum range. Particles are detected in six identical magnetic spectrometers based on a six-coil, superconducting toroidal magnet. Each spectrometer (sector of the forward detector) will be equipped with a forward vertex tracker (FVT) and a set of drift chambers (FDC) for tracking, a high-threshold Cherenkov counter (HTCC) for electron identification, a low-threshold Cherenkov counter (LTCC) for pion identification, scintillation counters (FTOF) for time-of-flight, and electromagnetic calorimeters (FEC).

Particles in the CLAS12 forward detector are detected and identified by measuring their momenta, time-of-flights, number of photons produced in threshold Cherenkov counters, and energy losses in the calorimeters and scintillator counters. Because the momenta of particles pK^+K^- relevant for this experiment are all below 3 GeV, time-of-flight is sufficient to detect

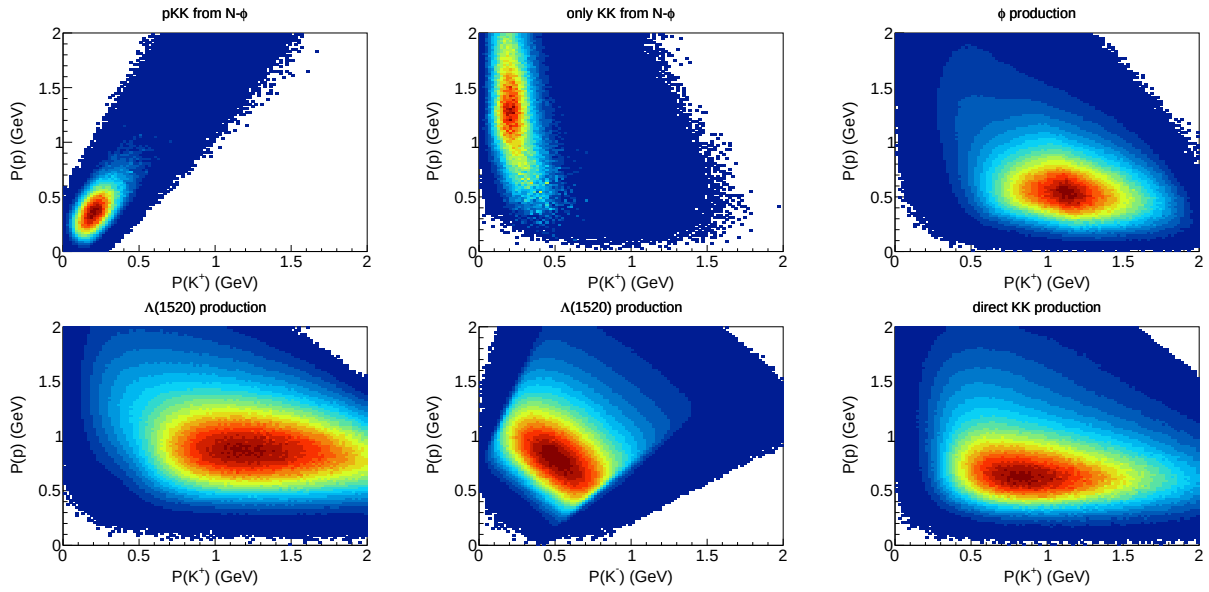

Figure 5: The proton-kaon momenta distributions from different channels. The upper left panel shows the momenta distribution of the proton and kaon decayed from the bound state. The upper middle panel shows the momenta distribution of the proton associated with the bound state production and the kaon decayed from the bound state. The upper right panel shows the distribution of the proton associated with the ϕ production and the kaon decayed from the ϕ. The lower left panel shows the distribution of the proton decayed from $\Lambda(1520)$ and the K^+ associated with the $\Lambda(1520)$ production. The lower middle panel shows the distribution of the proton and K^- decayed from the $\Lambda(1520)$. The lower right channel shows the distribution of the proton and kaon from direct two kaons productions. All spectra in these plots are produced with electron beam energy 4.4 GeV on a 0.01 mm gold foil target, scattered electrons between 2.5 deg and 4.5 deg and between 1 GeV and 4 GeV and 3e34cm^{-2}s^{-1}luminosity.

Table 1: CLAS12 and Forward tagger design characteristics.

Parameters	Forward Detector	Central Detector	Forward Tagger
Charged Particles:			
Polar Angular Range (θ)	5° to 35°	35° to 125°	2.5° to 4.5°
Resolution:			
Polar Angle ($\delta\theta$)	$<$ 1 mrad	$<$ 10 mrad to 20 mrad	$<$ 1.5%
Azimuthal Angle ($\delta\phi$)	$<$ 4 mrad	$<$ 5 mrad	$<$ 2°
Momentum (δp/p)	$<$ 1% at 5 GeV/c	$<$ 5% at 1.5 GeV/c	$< 0.02/\sqrt{(E)}$
Neutral Particles:			
Polar Angular Range (θ)	5° to 40°	40° to 125° (neutrons)	
Resolution:			
Polar angle ($\delta\theta$)	$<$ 4 mrad	$<$ 10 mrad	
Energy	$< 0.1/\sqrt{(E)}$	$<$ 5%	
PID:			
e/π	full momentum range	N/A	full momentum range
π/p	full momentum range	$<$ 1.25 GeV/c	
K/π	$<$ 3 GeV/c	$<$ 0.65 GeV/c	
K/p	$<$ 4 GeV/c	$<$ 1 GeV/c	

them.

The CLAS12 forward tagger consists of a scintillatior hodoscope, a MicroMega tracker and a PbWO EM calorimeter and covers from 2.5° to 4.5° in polar angle. The scattered electrons are detected to ensure that the reaction is quasi-real photo-production. The forward tagger has performed very well since the CLAS12 Run Group A started to collect data in Spring 2018 both as an electron detector and part of the level-1 trigger in coincidence with CLAS12 main detectors.

3.3 ALERT Detector

3.3.1 Overview of the ALERT Design

The already approved low energy recoil detector consists of two sub-systems: a drift chamber and a scintillator hodoscope. As described in the Ref. [57], The drift chamber will be composed of 8 layers of sense wires to provide track information while the scintillators will primarily provide particle identification. The scintillator hodoscope will be placed inside the gas chamber, just outside of the last layer of drift wires, to reduce the material budget and reduce the energy threshold for detecting recoil particles as low as possible.

The detector is designed to fit inside the central TOF of CLAS12; the silicon vertex tracker and the micromegas vertex tracker (MVT) will be removed. The available space has

thus an outer radius of 20 cm. A schematic layout of the preliminary design is shown in Figure 6. The different detection elements are all covering about 340° of the polar angle to leave room for mechanics, and are 30 cm long with an effort made to reduce the particle energy loss through the materials. It is composed of:

- The target cell;
- A clear space filled with helium to reduce secondary scattering from the high rate Møller electrons. Its outer radius is 30 mm;
- The drift chamber (DC), its inner radius is 32 mm and its outer radius is 85 mm. It will detect the trajectory of the low energy nuclear recoils;
- Two rings of plastic scintillators placed inside the gaseous chamber, with total thickness of roughly 20 mm.

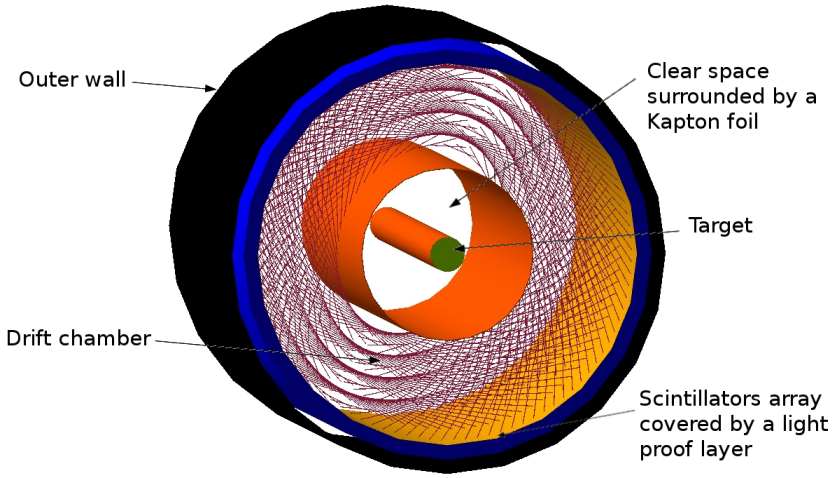

Figure 6: The schematic layout of the ALERT detector design, viewed from the beam direction. This figure is from Ref. [57].

The target cell in the original ALERT group proposal is a 30 cm long cylinder with an outer radius of 6 mm and target walls 25 μm Kapton filled with deuteron or helium gas. We will keep almost the same structure of the original ALERT target cell in this proposal, but with the end caps removed. A removable 0.1 mm gold foil will be placed at the upstream entrance of the Kapton cylinder to maximize the detection acceptance of the recoil protons and kaons.

The drift chamber volume will be filled with a light gas mixture (90% He and 10% C_4H_{10}) at atmospheric pressure. The amplification potential will be kept low enough in order not to be sensitive to relativistic particles such as electrons and pions. Furthermore, a light gas

mixture will increase the drift speed of electrons created during the ionization. This will allow the chamber to withstand higher rates due to a shorter hit occupancy time window. Based on these characteristics, the signals from this chamber and the scintillators could be used in coincidence with the electron trigger to reduce the DAQ trigger rate and allowing for operation at increased luminosity.

The proposed cylindrical drift chamber is 30 cm long, and for which the space between wires is around 2.0 mm. The radial form of the detector does not allow for 90 degrees x-y wires in the chamber. Thus, the wires of each layer are at alternating angle of $\pm 10°$, called the stereo-angle, from the axis of the drift chamber. The stereo-angles between wires are used to determine the coordinate along the beam axis (z). The drift chamber cells are composed of one sense wire made of gold plated tungsten surrounded by field wires, however the presence of the 5T magnetic field complicates the field lines. The cell configurations have been studied with MAGBOLTZ [58] by the ALERT group and will be tested in a prototype. A conservative configuration chosen by the ALERT group, in which the sense wire is surrounded by 6 field wires placed equidistantly from it in a hexagonal pattern, has been studied with the simulation code MAGBOLTZ. Assuming a conservative 10 ns time resolution, the spatial resolution is expected to be around 200 microns due to field distortions and spread of the signal. And the maximum occupancy of the drift chamber is expected to be of 5% for the inner most wires at 10^{35} $\mathrm{cm}^{-2}\mathrm{s}^{-1}$.

The read-out options of the signals from the wires have been considered by ALERT group. Currently the plan is to use the electronics used by the micromegas vertex tracker of CLAS12, known as the DREAM chip [59]. Its dynamic range and time resolution correspond to the needs of this drift chamber. To ensure that it is the case, tests with a prototype will be performed at the IPN Orsay (see section 3.5 in Ref. [57]).

The scintillator array will serve two main purposes. First, it will provide a useful complementary trigger signal because of its very fast response time, which will reduce the random background triggers. Second, it will provide particle identification, primarily through a time-of-flight measurement, but also by a measurement of the particle total energy deposited and path length in the scintillator which is important for doubly charged ions.

The length of the scintillators cannot exceed roughly 40 cm to keep the time resolution below 150 ps. It must also be segmented to match with tracks reconstructed in the drift chamber. The initial scintillator design of the ALERT group consists of a thin (2 mm) inner layer of 60 bars, 30 cm in length, and 600 segmented outer scintillators (10 segments 3 cm long for each inner bar) wrapped around the drift chamber. Each of these thin inner bars has silicon photomultiplier (SiPM) detectors attached to both ends. A thicker outer layer (18 mm) will be further segmented along the beam axis to provide position information and maintain good time resolution. For the outer layer, a SiPM will be mounted directly on the outer layer of a keystone shaped scintillator that is 30 mm in length and 18 mm thick. This design can be seen in Figure 7 which shows a full Geant4 simulation of the drift chamber and scintillators. By directly mounting the SiPMs to the scintillator, maximum signal is

collected in the shortest amount of time and the time resolution of SiPMs is expected to be a few tens of ps, which is well within the design target.

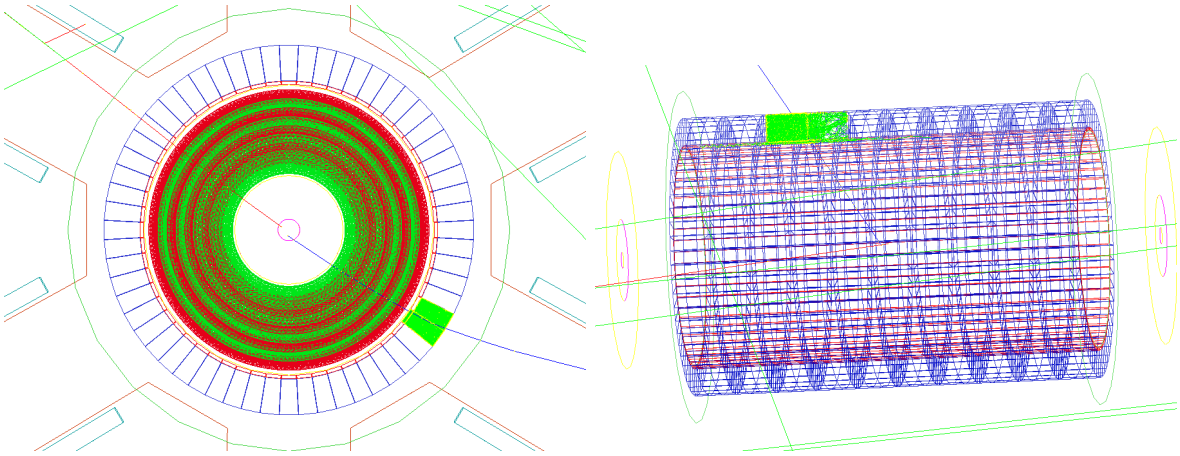

Figure 7: Geant4 simulation of a proton passing through the recoil drift chamber and scintillator hodoscope. The view looking downstream (left) shows the drift chamber's eight alternating layers of wires (green and red) surrounded by the two layers of scintillator (red and blue). Simulating a proton through the detector, photons (green) are produced in a few scintillators. This figure is from Ref. [57].

The front-end electrons for the SiPMs will include preamplifiers and application-specific integrated circuit (ASICs) which provide both TDC and ADC readouts. The PETIROC-2A [60] ASIC provides excellent time resolution (18 ps on trigger output with 4 photoelectrons detected) and a maximum readout rate at about 40k events/s. Higher readout rates can be handled with external digitizers by using the analog mode of operation and this could increase the rate by an order of magnitude. The ASIC also has the advantage of being able to tune the individual over-bias voltages with an 8-bit DAC.

3.3.2 Reconstruction and Particle Identification

The general detection and reconstruction scheme for ALERT is as follows. Fitting a track with the drift chamber and scintillator position information yields a track radius which is proportional to the transverse momentum over the charge. Next, using the scintillator time-of-flight, the particles are separated and identified by their mass-to-charge ratio.

A Geant4 simulation package of the ALERT detector has been implemented with the full geometry and material specifications. It includes a 5 Tesla homogeneous solenoid field and the entire detector filled with materials as described in the previous section. We focus on the simulation of protons and kaons in this study. To do this, the recoil particles are

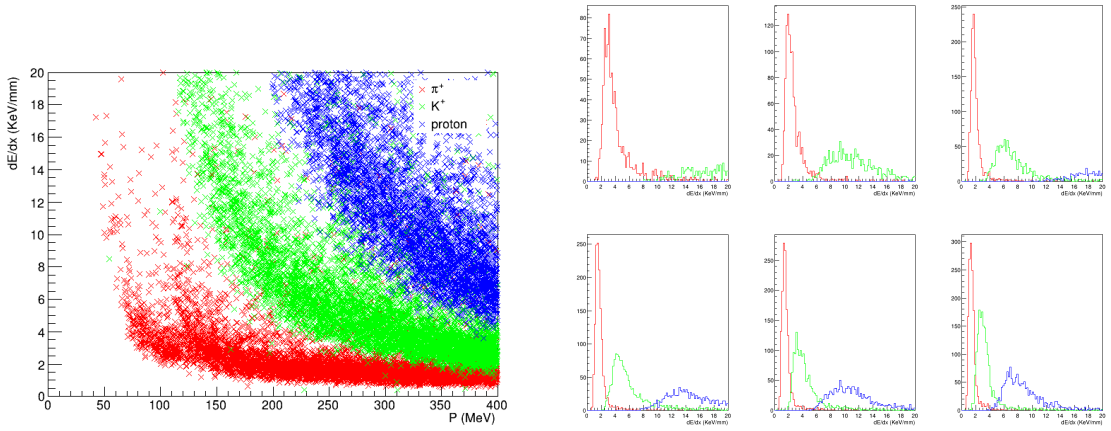

Figure 8: Simulated dE/dx in DC versus the momentum of the particle in 2D format(left plot) and 1D momentum bin from 100 MeV to 400 MeV with 50 MeV bin width (right plot). The color blue corresponds to proton, green to K^+ and red to π^+. Minimum Ionized Particles (MIPs) like electrons has a band below pions

generated with the same flat distributions: uniform in momentum from threshold to 400 MeV/c; isotropic angle coverage; flat distribution within the gold foil; and a radial vertex coordinate smeared around the beam line center by a Gaussian distribution of sigma equal to the expected beam radius (0.2 mm). We require that the particle reaches the scintillator and obtain the acceptance for protons and kaons as shown in Figure 9.

The gas mixture is changed from the ALERT detector default (90% He and 10% C_4H_{10}) to another common drift chamber gas (80% Ar and 20% C_4H_{10}). This is to increase the separation between kaon and pion and Minimum Ionized Particle (MIPs) like electrons in the drift chamber as shown in Fig. 8.

The tracks obtained from a helix fitter are used to determine the coordinates of the vertex and the momentum of the particles. The energy deposited in the scintillators can also be used to help determine the kinetic energy of the nucleus. The tracking capabilities of the recoil detector are investigated with the simulation. During the study, the spatial resolution of the drift chamber is assumed to be $\sim$200 μm and the stereo angle of the wires is assumed to be 10° in the z direction. The resulting differences between the generated and reconstructed kinematic variables from simulation are shown in Figure 10,Figure 11,Figure 12 for protons and K^+.

The particle identification scheme is investigated using the GEANT4 simulation as well. As mentioned in previous section, the scintillators have been designed to ensure a 150 ps time resolution. From Ref. [61], one can assume that with 8 hits in the drift chamber and the measurements in the scintillators, the energy resolution should be around 10% or better.

With this assumption, the particle identification property of the ALERT detector for

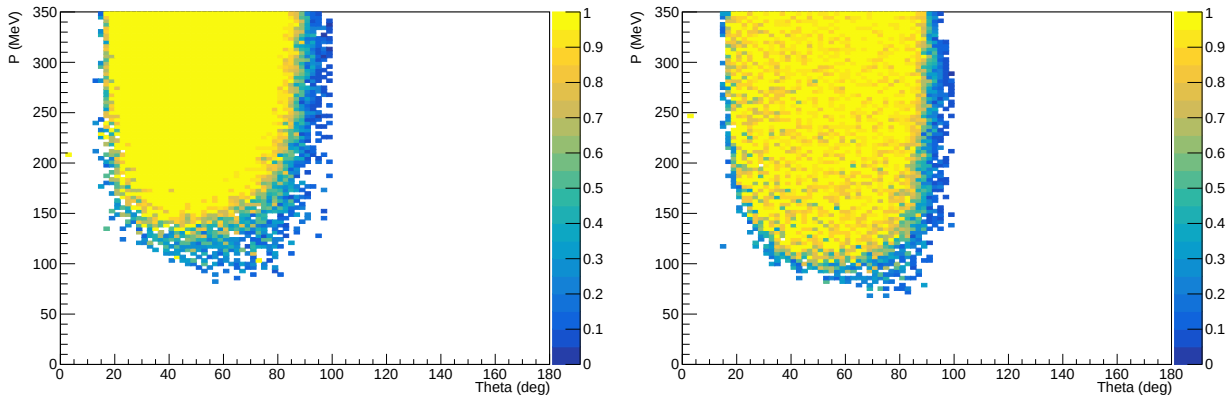

(a) Proton acceptance (b) K^+ acceptance

Figure 9: The momentum and angle acceptance of the ALERT detector for proton and K^+. The target is a thin gold foil located at the upstream entrance of the detector.

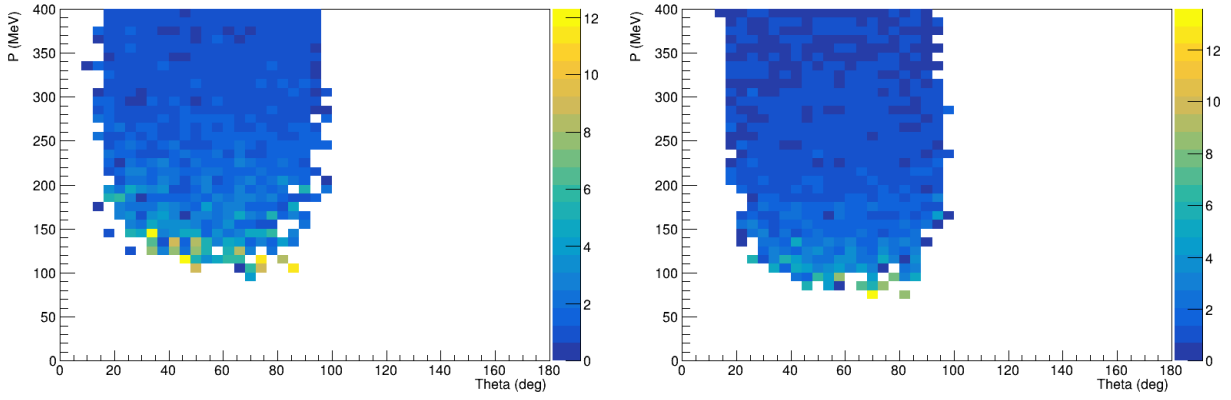

(a) Proton momentum resolution in percentage (b) K^+ momentum resolution in percentage

Figure 10: The simulated momentum resolutions within the momentum and polar angle coverage

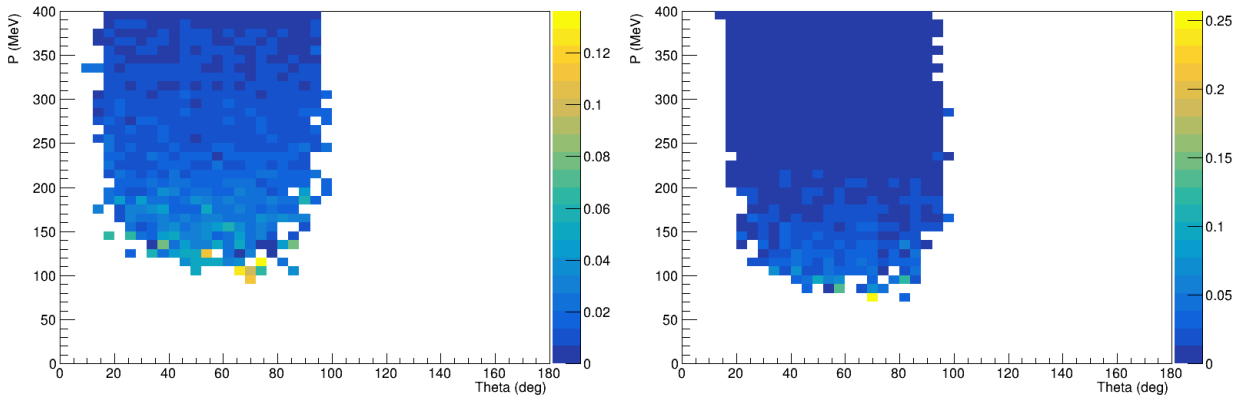

(a) Proton polar angle resolution in rad (b) K^+ polar angle resolution in rad

Figure 11: The simulated polar angle resolution within the momentum and polar angle coverage

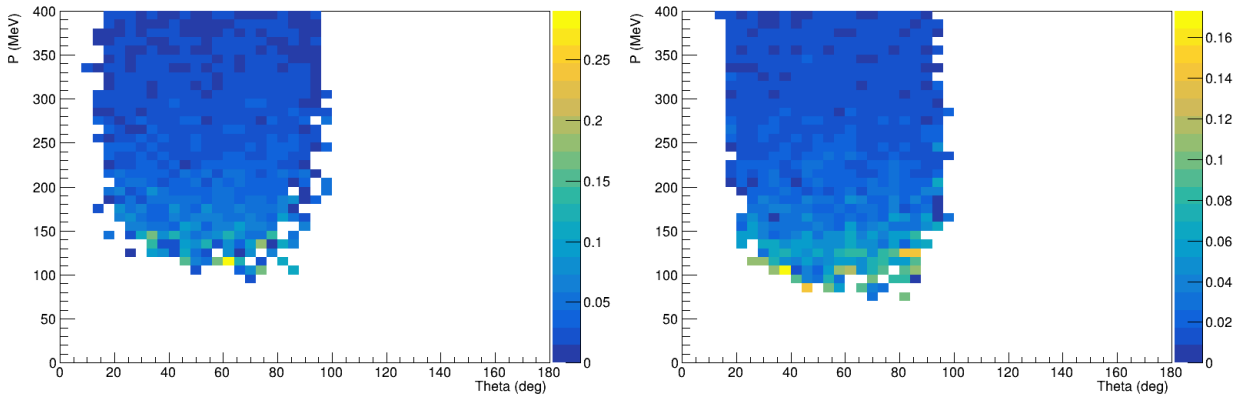

(a) Proton azimuthal angle resolution in rad (b) K^+ azimuthal angle resolution in rad

Figure 12: The simulated azimuthal angle resolution within the momentum and polar angle coverage

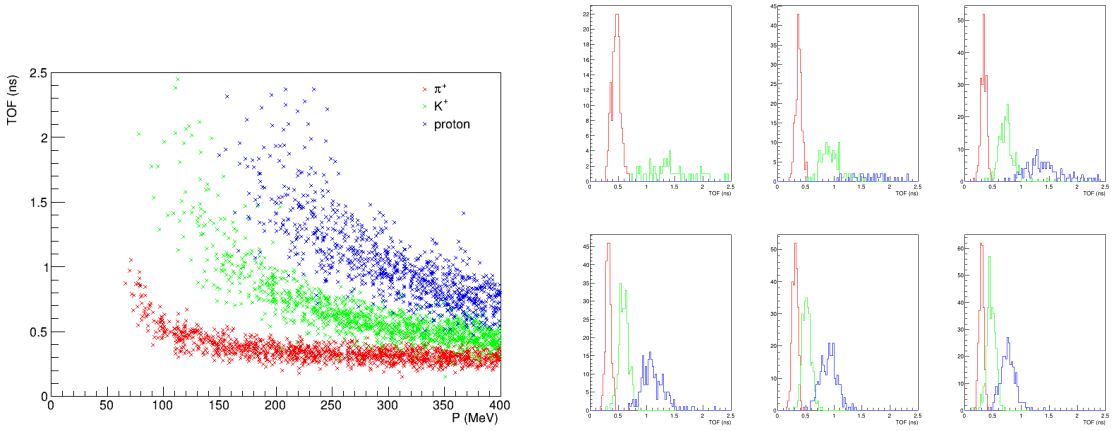

Figure 13: Simulated time-of-flight at the scintillator versus the reconstructed momentum of the particle in 2D format(left plot) and 1D momentum bin from 100 MeV to 400 MeV with 50 MeV bin width (right plot). The color blue corresponds to proton, green to K^+ and red to π^+. The reconstructed polar angle of the recoil particle is limited to the largest angle 75° $\sim$ 85° which has the shortest flight path. Other smaller angle will have longer flight path and better PID. The TOF in this plot has already been smeared by the 150 ps timing resolution of ALERT.

particles heavier than proton has been studied by the ALERT group in Ref. [57] and the result is pretty convincing. For this proposal we will only focus on the particle identification of protons and kaons. We plan to use the same TOF technique including both flight time information from scintillator and flight path length from tracking. Without apply the complete tracking algorithm to estimate flight path length, we can use a polar angle cut, which is directly related to flight path length, to check the result with simulation. The polar angle cut of ±5° is slightly above the typical Alert tracking resolution. We simulated an equal amount of protons, kaons as well as pions and obtained a particle identification, a clean separation of pions, kaons and protons up 350 MeV is shown in the 2D plot of 13 for the largest angle 75° $\sim$ 85° which has the shortest flight path. Other smaller angle will have longer flight path and even better PID. The TOF of the particles has been smeared by a Gaussian-shape resolution function with σ equals to 150 ps, which is the timing resolution of the scintillator in the original ALERT proposal. To quantify the separation power, we show the 1D plot of 13 which covers from 100 MeV to 400MeV in 50 MeV bin. Then we apply a cut to check the resulting pion rejection and kaon efficiency. By tuning the momentum dependent cut values, we obtain better than 100 pion rejection from 100 MeV to 300 MeV, while kaon efficiency changes from 100% to 96%. Between 300 MeV and 350 MeV, pion rejection is 65 and kaon efficiency is 90%. And between 350 MeV and 400 MeV, pion rejection is 40 and kaon efficiency drops to 80%. To be conservative, for this proposal, we consider kaon and proton only can be identified below 350 MeV and we use pion rejection 50 for our background study in the following section.

This analysis suggests that the proposed reconstruction and particle identification schemes for this design are quite promising. Studies, using both software and prototyping, are ongoing to determine the optimal detector parameters to minimize the detection threshold while maximizing particle identification efficiency.

For this proposal, ALERT can detect charged kaon and proton between 100 MeV and 350 MeV and from 20° to 90° with good resolution. Its offline pion rejection can reach 50. A single particle (kaon or proton) detection efficiency including both DC and scintillator are assumed to be 90% each. For three final particles, we have 70% overall detection efficiency.

4 Proposed Measurements

4.1 Overview

Enlightened by the physics motivations presented in the previous sections and the kaon PID capability of the already approved ALERT detector, we propose to search for the $\phi - N$ bound state by measuring its dominant pK^+K^- decay channel combining the CLAS12 forward detector, the Forward Tagger, and the ALERT detector.

A 4.4 GeV electron beam energy with 42 nA current incident on a 0.1 mm thickness gold foil target will be used for the search. We choose a large current and a thin target to minimize the final particle energy loss in the target material and keep the luminosity at the ALERT limit of 3e34 $cm^{-2}s^{-1}$. The foil target is placed at the upstream end of the 30 cm long ALERT detector, which is the -15 cm upstream of the CLAS12 center. This is to optimize the forward angle detection where most of the signal events are. The three final state particles of the dominant pK^+K^- decay channel with a suggested branching ratio of 46.5% will be detected by the CLAS12 forward detector and the ALERT detector. The scattered electron will be detected by the Forward Tagger to ensure that it is a quasi-real photo-production.

4.2 Simulation

After signal and background events are generated as mentioned in Section 3.1, all final state particles go through a fast Monte-Carlo simulation to include all detector acceptance and resolution effect. The electrons detected by the forward tagger are required to be with 2.5 and 4.5 deg and above 1 GeV, which is included in the event generation. The acceptance of the recoil proton and kaons by CLAS12 forward angle detectors is based on and the CLAS12 fast simulation. Their acceptance by ALERT is base on result of full Geant4 simulation described in Section 3.3.2 and represented in Figure 9. Kaons that decay before reaching the detector, CLAS12 or ALERT, are not counted. The particle energy lose in the target is taken into account based on the stopping power data by NIST, though the effect is negligible since the gold foil target is thin. The momenta of detected particles are smeared with gaussian distributions according to detector resolutions. For CLAS12 forward detector, we use averaged 1% momentum amplitude, 1 mrad polar angle and 4 mrad azimuthal angular resolutions. For ALERT, we use the simulated resolution distribution from Figure 10,Figure 11,Figure 12.

Combining the generated signal events with the detector acceptances and resolutions through simulation, the invariant mass spectra of the detected pK^+K^- from the signal and correlated background channels is shown in Figure 14.

The momentum-polar angle distributions of the detected proton and kaons from the

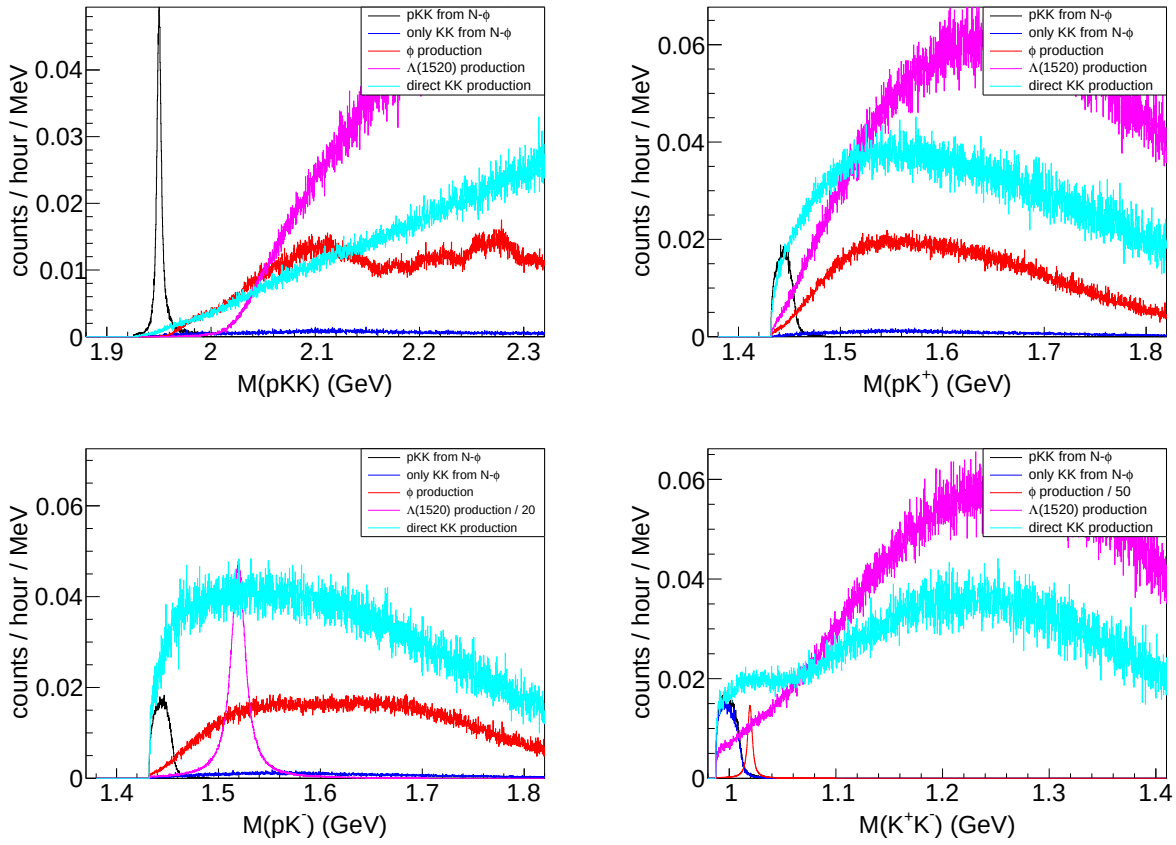

Figure 14: The invariant mass of detected pK^+K^- (upper left), pK^+ (upper right), pK^- (lower left) and K^+K^- (lower right) from the signal and correlated background channels. Comparing to Figure 3, detector acceptance and resolution are added.

bound state are shown in Figure 15. A major portion of signal events is detected by the ALERT detector. CLAS12 forward angle detector can't cover large angle and also loses many kaons due to their decay before they reach the FTOF detector more than 6 m away. There is a gap in momentum between CLAS12 forward angle and ALERT which can be further optimized by tuning CLAS12 torus field strength.

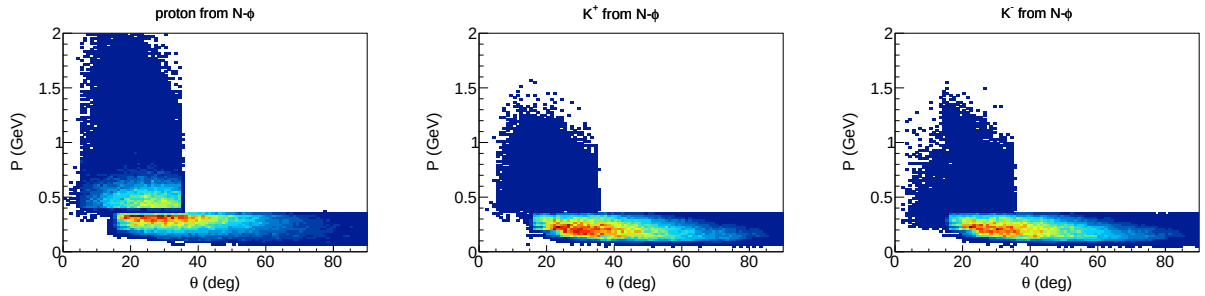

Figure 15: The momentum-polar angle distributions of the detected proton and kaons from the bound state. The left panel is the distribution of the detected proton, the middle panel is the distribution of the detected K^+, and the right panel is the distribution of the detected K^-. Comparing to Figure 4, detector acceptance and resolution are added. The particles with momentum less than 350 MeV are detected by the ALERT detector and all the other particles are detected by CLAS12 Forward detector.

The momentum distributions of the detected proton and kaons from the signal channel and correlated background channels mentioned above are shown in Figure 16. We can reduce the background by removing high momentum events, and we apply the momentum cuts $P(p) < 0.8$ GeV and $P(K^{\pm}) < 0.5$ GeV. In addition, we can apply cuts on the invariant mass $M(pK)$ and $M(KK)$ to further reduce the background as can be observed in Figure 14, and we apply the invariant mass cuts $M(pK^{\pm}) < 1.48$ GeV and $M(K^+K^-) < 1.04$ GeV. The invariant mass spectra of correlated pK^+K^- after these cuts are shown in Figure 17. After those cuts, the correlated pK^+K^- background channels studied here are very small comparing to the signal channel.

In additional the correlated pK^+K^- background channels, we also consider a spectator proton broken loose from the nuclei being detected, instead of the proton participating the reaction. We call it the uncorrelated pK^+K^- background channels. Because we do not detect the signal channel exclusively, there could be other more complicated final states. So to be conservative, we give these uncorrelated channels crosssection as large as the correlated channels. The invariant mass of the detected pK^+K^- from the signal and the uncorrelated background channels are shown in Figure 17. One additional cut of the detected proton polar angle $< 60°$ helps reduce those uncorrelated background while the signal channel is only reduced by 5%. The background from the uncorrelated background is about 35% of the signal channel after the cut and we consider them in the projection and beam request.

Apart from the pK^+K^- background channels, there could be major background from the

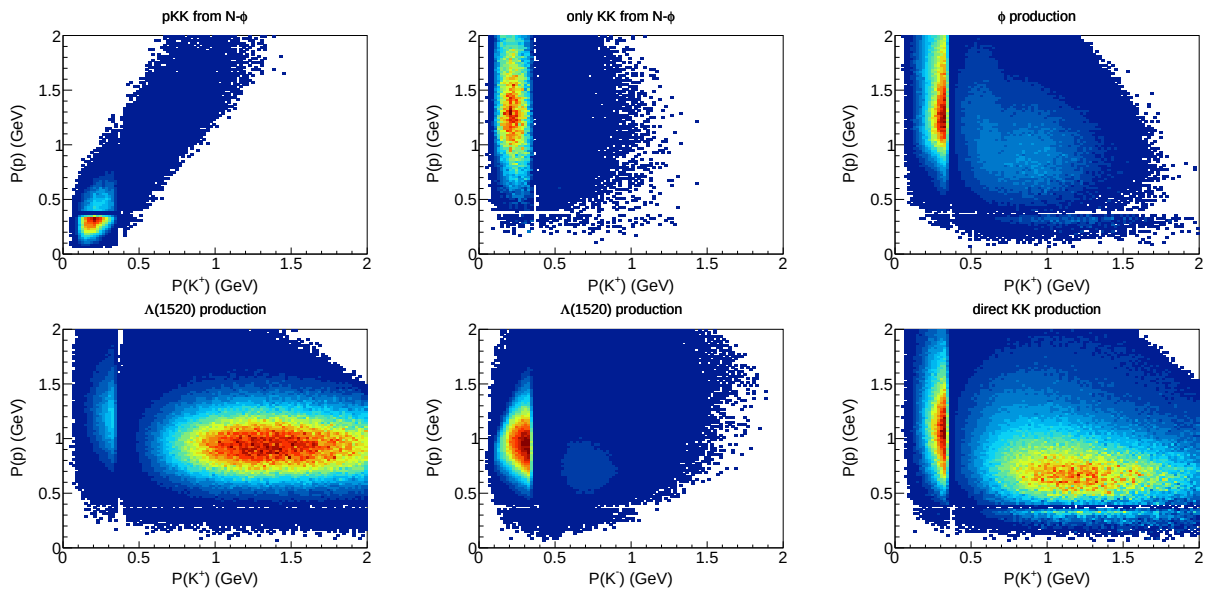

Figure 16: The momenta distributions of detected protons and kaons from the signal and correlated background channels. Comparing to Figure 5, detector acceptance and resolution are added.

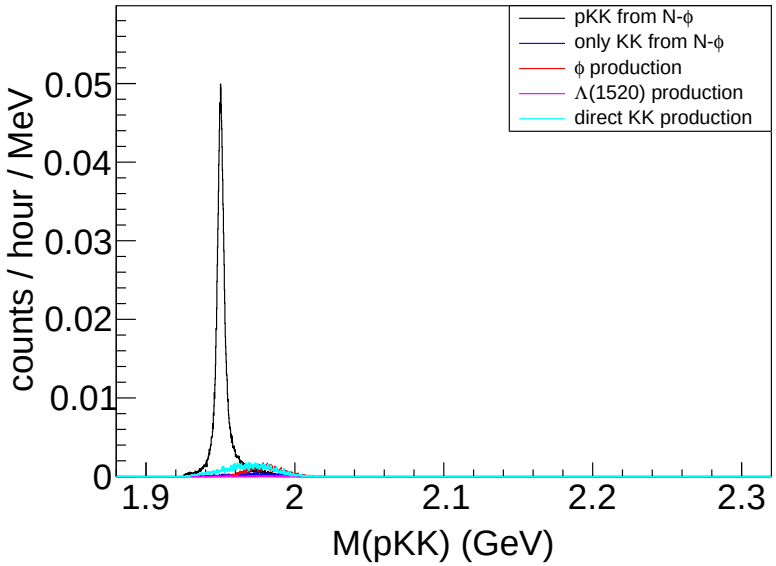

Figure 17: The invariant mass of the detected pK^+K^- from the signal and **correlated background channels**, after a set of cuts: $P(p) < 0.8$ GeV, $P(K^{\pm}) < 0.5$ GeV, $M(pK^{\pm}) < 1.48$ GeV, and $M(K^+K^-) < 1.04$ GeV. The count rate is normalized with 3e34 $\mathrm{cm}^{-2}\mathrm{s}^{-1}$luminosity.

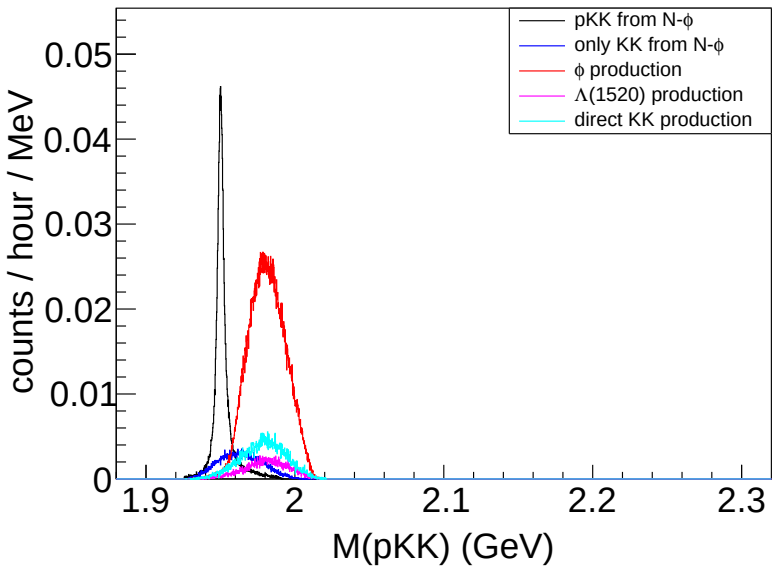

Figure 18: The invariant mass of the detected pK^+K^- from the signal and **uncorrelated background channels**, after a set of cuts: $P(p) < 0.8$ GeV, $P(K^{\pm}) < 0.5$ GeV, $M(pK^{\pm}) < 1.48$ GeV, $M(K^+K^-) < 1.04$ GeV, and **additional cut** $P(p) < 60^\circ$. The count rate is normalized with 3e34 $\mathrm{cm}^{-2}\mathrm{s}^{-1}$luminosity.

exclusive $p\pi^+\pi^-$ channel if both pion are misidentifed as kaons, because the cross sections for the two pion exclusive production is much larger than those of kaon productions. We used the new event generator TWOPEG [62] to estimate the two pion exclusive production crosssection. It is based on a model fit to all results on charged double pion photo- and electroproduction cross sections from CLAS with some extrapolation. It covers a kinematical area in Q2 starting from 0.0005 GeV2 and in W from the reaction threshold up to 4.5 GeV, which are much larger than this proposal's coverage. The generator has already been used in CLAS data analyses and in PAC proposal preparations and is designed to be used during the CLAS12 era.

We put the generated exclusive two pion events through the same simulation like the two kaon channels to check how it affects the background. The addtional thing to consider is that dominate number of events are detected by ALERT detector and it has good pion rejection as high as 100 based on the simulation described in Section 3.3. Thus we assume that conservative rejection factor 50 or 2% pions are misidentified as kaons. After applying the same set of cuts like the two kaon channels, the comparison between the signal channel and the two pion background is shown in Figure 19. The background from exclusive two pion channel is about twice as much as the signal and we take it into account when considering project and beam request.

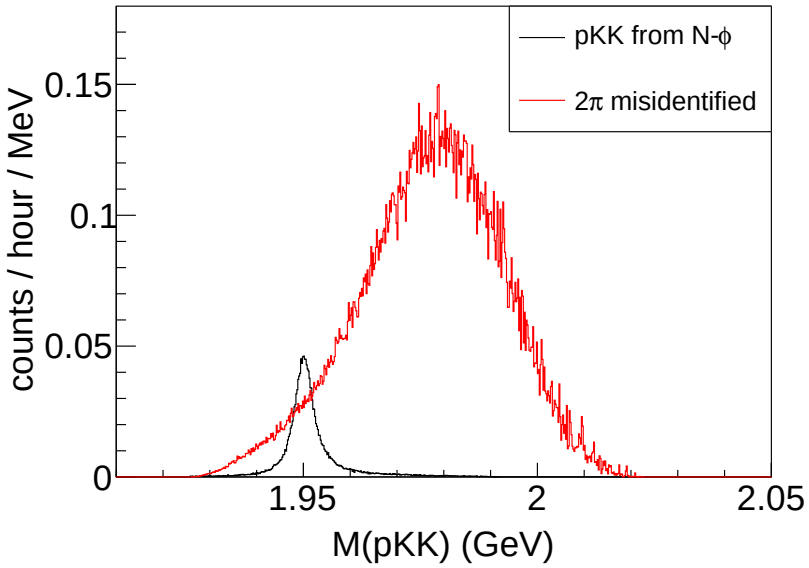

Figure 19: The comparison between the invariant mass distribution of the pK^+K^- from the bound state (black) and the exclusive $p\pi^+\pi^-$ production with both pions misidentified as kaons (red). We have applied the same set of cut as in Figure 18. The count rate is normalized with 3e34 $\mathrm{cm}^{-2}\mathrm{s}^{-1}$luminosity.

4.3 Project and Beam Request

Based on the simulation, we can select the $\pm 3\sigma$ (dominated by detector resolution) region $1940\,\mathrm{MeV} < M(pK^+K^-) < 1960\,\mathrm{MeV}$ to estimate signal and the main background from exclusive two-pions production. We assume 3e34 $\mathrm{cm}^{-2}\mathrm{s}^{-1}$luminosity and 70% overall detection efficiency (each final particle 90%). The signal rate is 0.2/h, the background from correlated pK^+K^- channel has negligible rate, the background from uncorrelated pK^+K^- channel has rate 0.07/h and the misidentified two-pions background rate is 0.43/h. For 40 days or 960 hours production beam time, we expect to have 192 signal events and 480 background events. So the excess is expected to be about 7.4σ $(= 192/\sqrt{192+480})$.

We request a total 45 days beam time, including 40 days for production and 5 days for calibration and commissioning of the detectors, to search for this bound state.

5 Summary

In summary, we propose to carry out a search of a $\phi - N$ bound state by performing a measurement of quasi-real photo-production of the possible $\phi - N$ bound state with its predicted mass near 1950 MeV and a 4 MeV total decay width. In order to perform this measurement, we propose to use the already approved low energy recoil detector ALERT to fit our experimental needs. The detector is designed such that it will provide relatively good timing resolution and particle identification. Together with the hidden charm pentaquark candidates discovered by LHCb, the investigations of this hidden strange pentaquark candidate may unravel the flavor dependent properties and the structures of multi-quark states.

In order to achieve the goals presented in this proposal, we request 45 days of running with 42 nA and 4.4 GeV electron beam on a 0.1mm gold foil target with a luminosity of 3e34 $\mathrm{cm}^{-2}\mathrm{s}^{-1}$. Among the requested 45 days, 40 days will be used for production and 5 days for calibration and commissioning of the detectors.

The ability of detecting low momentum kaons is also valuable for other experiments such as the Very Strange experiment that aims for the study of $S = -2$ and $S = -3$ baryons rates. These states are produced in association with multiple kaons in the final state, and the capability of the future ALERT detector would greatly improve the reconstruction efficiencies for reactions such as $ep \to eK^+K^+K^-\Lambda$, searching for excited cascades, etc.

6 Appendix

6.1 Summary of Conditions

Here is a short summary of conditions of experimental setup and simulation projection, which this proposal is based on.

Experimental setup conditions:

1. CLAS12 forward angle detector and ALERT detector to detect proton and chargded kaons and forward tagger to detect scattering electrons.

2. 0.1mm gold foil target at z=-15cm with 4.4 GeV electron beam and the luminosity is 3e34 $\mathrm{cm}^{-2}\mathrm{s}^{-1}$.

Simulation projection conditions:

1. the $\phi-N$ bound state production and decay model with quasi-real electron production on thin gold foil is based on Ref. [14]. The production has two step processes where the first step of ϕ production involves a neutron or a proton and the second step of forming the bound state involves a proton only. The decay has 46.5% branching ratio into pK^+K^-. The

detection of the final state pK^+K^- from the bound state doesn't exclude other production and decay models

2. Several correlated background channels with the same pK^+K^- final states are studied and spectator protons are considered as uncorrelated backgrounds. The two-pion exclusive background is also taken into account.

3. Forward Tagger covers 1 - 4 GeV in energy and 2.5 - 4.5 deg in polar angle.

4. The CLAS12 forward angle detector acceptance and resolution are based on its fast simulation.

5. Based on the ALERT Geant4 simulation, ALERT detector covers 100-350 MeV in momentum and 20 to 90 deg in polar angle. Its tracking and timing solution are simulated for PID and smearing kinematic variables. The expected pion rejection factor is 50 on average.

6. Cuts applied to reduce various backgrounds are $P(p) < 0.8$ GeV, $P(K^{\pm}) < 0.5$ GeV, $M(pK^{\pm}) < 1.48$ GeV, $M(K^+K^-) < 1.04$ GeV, and $P(p) < 60°$.

7. The overall efficiency of the pK^+K^- final state is assumed to be 70%.

6.2 Trigger

This proposal needs to detect e- on CLAS12 Forward Tagger (FT) and proton, K+,K- on ALERT or CLAS12 forward angle detector (FD)

As there is actual data taking with the exact same condition of this proposal, we estimate Forward Tagger trigger rate based on a real run with close condition and physics considerations. The Forward Tagger single-cluster trigger rate for run 3048 has ∼70 kHz rate with 15 nA 6.4 GeV electron beams on 5cm long liquid hydrogen target (luminosity 2e34/cm2/s) and 0.5 GeV threshold. The quasi-real virtual photon has minimum $Q^2 = 0.006\,\mathrm{GeV}^2$. For this proposal, the running condition would be 42 nA 4.4 GeV electron beam on 0.1 mm thick gold foil target and threshold 1GeV on the Forward Tagger (We also cut below 4 GeV to remove elastic/quasi-elastic contribution), The minimum $Q^2 = 0.008\,\mathrm{GeV}^2$ is a factor 1.33 larger and the luminosity 3e34/cm2/s is a factor of 1.5 larger. Assuming the rate is proportional to virtual photon flux ($\propto E'/Q^2E$) and luminosity, the expected Forward Tagger single-cluster trigger rate is 238 kHz (=3.4*70).

To keep the trigger rate within the current CLAS12 limit of 12kHz, and assume 50 ns coincidence trigger time window, we need to have CLAS12 forward angle detector and ALERT provide a combined single particle trigger to preserve charged kaon and protons with a trigger rate below 1 MHz.

The coincidence trigger between CLAS12 forward angle detector and forward tagger are commonly used. The ALERT detector can provide a trigger using its DC electronics and

scintillators electronics as a binary value for threshold and multiplicity.

If approved, we will contribute to the design and implementation of ALERT trigger with CLAS12 trigger system.

6.3 Changes to ALERT Detector

This proposal plans to use ALERT detector with small changes and has different run conditions. Here we summarize the changes from standard ALERT runs.

1. using a thin gold foil target at the entrance of ALERT instead of Alert default gas target.

2. using gas mixture of 80% Ar + 20% C4H10 instead of ALERT default DC gas, for better separation between kaon and pion/MIP. The ALERT DC threshold may change accordingly.

3. Put ALERT and CLAS12 forward angle detector in trigger to do coincidence trigger with forward tagger so that we can stay within the CLAS12 trigger rate limit.

Please note the we will keep the same luminosity 3e34 $cm^{-2}s^{-1}$as ALERT experiment has.

6.4 Other Options for a Low Energy Recoil Detector

6.4.1 CLAS12 Central Detector

The CLAS12 Central Detector [56] is designed to detect various charged particles over a wide momentum and angular range, which includes:

- Solenoid Magnet: provides a central longitudinal magnetic field up to 5 Tesla; it will be used by the ALERT detector to suppress the low energy electrons and determine the momentum of the particles through tracking.
- Central Tracker: consists of 3 layers of silicon strips with 300 μm thickness for each layer and 3 layers of Micromegas.
- Central Time-of-Flight: a cylinder consists of an array of scintillator paddles with radius 26 cm and length 50 cm; the thickness of the scintillator paddle is 2 cm; the designed timing resolution is 50 ps; it is used to separate pions and protons up to 1.2 GeV/c.

We do not plan to use the CLAS12 central detector because it is not suitable for our measurements of the low energy particles ($p < 300$ MeV/c) due to the energy loss in the first

2 silicon strip layers. The momentum detection threshold is ∼200 MeV/c for protons which is significantly too large for our proposed measurements.

6.4.2 BoNuS12 Radial Time Projection Chamber

The BoNuS12 cylindrical radial time projection chamber (RTPC) is being developed for experiment E12-06-113 [63], which is based on the successful cylindrical RTPC built for experiment E03-012 [64]. The sensitive drift region of the RTPC is a 40 cm long annulus with the inner radius of 30 mm and outer radius of 70 mm, filled with a mixture of 82% He gas and 18% dimethyl ether gas. The amplification of the drifting electrons is achieved by three layers of cylindrical Gas Electron Multiplier (GEM, see [65]) foils at radii of 70, 73 and 76 mm. The foils are surrounded by a cylindrical readout surface featuring rectangular pads at a radius of 78 mm. The GEMs are 50 μm thick polyamide foils coated on both sides with a 5 μm copper layer and punctured with 70 μm holes. By applying a voltage in the range of 200 V to 300 V across the two copper layers a very high electric yield is formed inside the holes. Ionized electrons drifting towards the GEM foil will produce an avalanche of secondary electrons when captured and accelerated through the holes. The maximum drifting time in the RTPC is ∼7 μs. After passing three GEM foils, the resulting electron pulse will be detected on the readout plane. Materials between the target and the sensitive detector volume are minimized to prevent energy loss of the recoiled particles and to minimize the interaction of background particles.

The BoNuS12 detector will be located inside the CLAS12 5T superconducting solenoid magnet. The track of the particle is fitted by a pattern-recognition algorithm from the hits reconstructed with the position and the drifting time recorded in the readout system. The momentum and the charge of the particle can be calculated from the curvature and polar angle of the track and the magnetic field. In combination with the measured momentum, energy deposit of the particle ($\mathrm{d}E\,/\,\mathrm{d}x$) derived from the signal pulse heights can be used to provide particle identification.

A Geant4 simulation package of the BoNuS12 detector was set up to determine the kinematic coverage and the particle identification. In the simulation, the gold foil target is located at the upstream edge of the detector to maximize the forward angle acceptance. Particles have been produced at angle $\theta = 0 \sim 100^\circ$ with momentum $p = 0 \sim 350$ MeV/c. shows the momentum and angle acceptance for p and K^+. The step-by-step information along the particle tracks produced by the simulation have also been analyzed to determine the $\mathrm{d}E\,/\,\mathrm{d}x$ in the detector for p, K^+ and π^+. Figure 20 displays the $\mathrm{d}E\,/\,\mathrm{d}x$ for each particle in our simulated momentum range. We expect kaons and protons can be identified below 250 MeV and pions can be suppressed with at least a factor of 10.

The issue with the RTPC is its slow response time due to the long drift time and thus it could not be included in the trigger effectively. In the BoNuS runs in CLAS, the data acquisition speed was the main limiting factor for higher luminosities. It would be a sig-

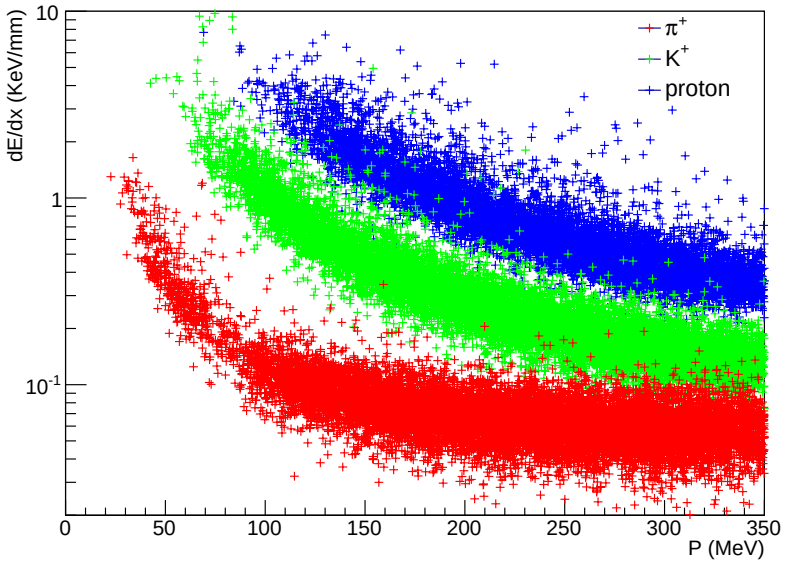

Figure 20: $\mathrm{d}E\,/\,\mathrm{d}x$ for p, K^+ and π^+ with momentum $p = 0 - 350$ MeV/c detected in the drift region of the RTPC.

nificant impact on the background rejection if the recoil detector could be included in the trigger since under most circumstances the recoil particles are not able to get out of the target region to be detected due to their too low momentum or too small angle. Including the recoil detector in the trigger would significantly reduce the trigger's frequency.

References

[1] M. Gell-Mann, Phys. Lett. **8**, 214 (1964).

[2] R. Aaij et al. (LHCb Collaboration), Phys. Rev. Lett. **115**, 072001 (2015).

[3] R. Aaij et al. (LHCb Collaboration), arXiv: **1904.03947** (2019).

[4] H.-X. Chen, W. Chen, X. Liu, and S.-L. Zhu, Phys. Rept. **639**, 1 (2016).

[5] V. Kopeliovich and I. Potashnikova, Phys. Rev. **D93**, 074012 (2016).

[6] J. He, Phys. Rev. **D95**, 074031 (2017).

[7] H. Li, Z.-X. Wu, C.-S. An, and H. Chen, Chin. Phys. **C41**, 124104 (2017).

[8] H. Huang, X. Zhu, and J. Ping, Phys. Rev. **D97**, 094019 (2018).

[9] S. J. Brodsky, I. A. Schmidt, and G. F. de Teramond, Phys. Rev. Lett. **64**, 1011 (1990).

[10] M. E. Luke, A. V. Manohar, and M. J. Savage, Phys. Lett. **B288**, 355 (1992).

[11] S. R. Beane, E. Chang, S. D. Cohen, W. Detmold, H. W. Lin, K. Orginos, A. Parreño, and M. J. Savage, Phys. Rev. **D91**, 114503 (2015).

[12] H. Gao, T. S. H. Lee, and V. Marinov, Phys. Rev. **C63**, 022201 (2001).

[13] X. Qian et al., Phys. Lett. **B696**, 338 (2011).

[14] H. Gao, H. Huang, T. Liu, J. Ping, F. Wang, and Z. Zhao, Phys. Rev. **C95**, 055202 (2017).

[15] F. Huang, Z. Y. Zhang, and Y. W. Yu, Phys. Rev. **C73**, 025207 (2006).

[16] J. He, H. Huang, D.-Y. Chen, and X. Zhu, Phys. Rev. **D98**, 094019 (2018).

[17] S. Liska, H. Gao, W. Chen, and X. Qian, Phys. Rev. **C75**, 058201 (2007).

[18] R. S. Hayano and T. Hatsuda, Rev. Mod. Phys. **82**, 2949 (2010).

[19] P. Gubler and K. Ohtani, Phys. Rev. **D90**, 094002 (2014).

[20] X.-D. Ji, Phys. Rev. Lett. **74**, 1071 (1995).

[21] H. Gao, T. Liu, C. Peng, Z. Ye, and Z. Zhao, The Universe **3**, 18 (2015).

[22] A. Bottino, F. Donato, N. Fornengo, and S. Scopel, Astropart. Phys. **18**, 205 (2002).

[23] J. R. Ellis, K. A. Olive, and C. Savage, Phys. Rev. **D77**, 065026 (2008).

[24] J. Giedt, A. W. Thomas, and R. D. Young, Phys. Rev. Lett. **103**, 201802 (2009).

[25] G. E. Brown and M. Rho, Phys. Rev. Lett. **66**, 2720 (1991).

[26] T. Hatsuda and S. H. Lee, Phys. Rev. **C46**, R34 (1992).

[27] R. Muto et al. (KEK-PS-E325 Collaboration), Phys. Rev. Lett. **98**, 042501 (2007).

[28] J. J. Cobos-Martínez, K. Tsushima, G. Krein, and A. W. Thomas, Phys. Lett. **B771**, 113 (2017).

[29] T. Ishikawa et al., Phys. Lett. **B608**, 215 (2005).

[30] M. H. Wood et al. (CLAS Collaboration), Phys. Rev. Lett. **105**, 112301 (2010).

[31] A. Polyanskiy et al., Phys. Lett. **B695**, 74 (2011).

[32] J. Yamagata-Sekihara, D. Cabrera, M. J. Vicente Vacas, and S. Hirenzaki, Prog. Theor. Phys. **124**, 147 (2010).

[33] J. J. Cobos-Martínez, K. Tsushima, G. Krein, and A. W. Thomas, Phys. Rev. **C96**, 035201 (2017).

[34] T. Mibe et al. (LEPS Collaboration), Phys. Rev. Lett. **95**, 182001 (2005).

[35] B. Dey, C. A. Meyer, M. Bellis, and M. Williams (CLAS), Phys. Rev. **C89**, 055208 (2014), [Addendum: Phys. Rev.C90, no.1, 019901 (2014)].

[36] H. Seraydaryan et al. (CLAS Collaboration), Phys. Rev. **C89**, 055206 (2014).

[37] A. Kiswandhi, J.-J. Xie, and S. N. Yang, Phys. Lett. **B691**, 214 (2010).

[38] A. Kiswandhi and S. N. Yang, Phys. Rev. **C86**, 015203 (2012), [Erratum: Phys. Rev.C86, 019904 (2012)].

[39] A. Kiswandhi, S. N. Yang, and Y. B. Dong, Phys. Rev. **C94**, 015202 (2016).

[40] Z. Y. Zhang, Y. W. Yu, P. N. Shen, L. R. Dai, A. Faessler, and U. Straub, Nucl. Phys. **A625**, 59 (1997).

[41] F. Huang, D. Zhang, Z. Y. Zhang, and Y. W. Yu, Phys. Rev. **C71**, 064001 (2005).

[42] F. Huang and Z. Y. Zhang, Phys. Rev. **C72**, 068201 (2005).

[43] H. Huang, P. Xu, J. Ping, and F. Wang, Phys. Rev. **C84**, 064001 (2011).

[44] H. R. Pang, J. L. Ping, F. Wang, and J. T. Goldman, Phys. Rev. **C65**, 014003 (2002).

[45] J.-L. Ping, F. Wang, and J. T. Goldman, Phys. Rev. **C65**, 044003 (2002).

[46] J.-L. Ping, F. Wang, and J. T. Goldman, Nucl. Phys. **A657**, 95 (1999).

[47] G.-h. Wu, J.-L. Ping, L.-j. Teng, F. Wang, and J. T. Goldman, Nucl. Phys. **A673**, 279 (2000).

[48] J. L. Ping, H. X. Huang, H. R. Pang, F. Wang, and C. W. Wong, Phys. Rev. **C79**, 024001 (2009).

[49] M. Chen, H. Huang, J. Ping, and F. Wang, Phys. Rev. **C83**, 015202 (2011).

[50] H. Huang, J. Ping, and F. Wang, Phys. Rev. **C92**, 065202 (2015).

[51] H. Huang, C. Deng, J. Ping, and F. Wang, Eur. Phys. J. **C76**, 624 (2016).

[52] A. Valcarce, H. Garcilazo, F. Fernandez, and P. Gonzalez, Rept. Prog. Phys. **68**, 965 (2005).

[53] J. He, Phys. Rev. **C91**, 018201 (2015).

[54] K. Moriya et al. (CLAS Collaboration), Phys. Rev. **C88**, 045201 (2013), [Addendum: Phys. Rev. **C88**, 049902(2013)].

[55] D. Dutta et al. (JLab E91013), Phys. Rev. **C68**, 064603 (2003).

[56] *CLAS12 Technical Design Report*, https://www.jlab.org/Hall-B/clas12_tdr.pdf.

[57] K. Hafidi et al., *JLab PR12-17-012*, https://www.jlab.org/exp_prog/proposals/17/PR12-17-012.pdf.

[58] S. F. Biagi, Nucl. Instrum. Meth. **A421**, 234 (1999).

[59] D. Attie et al., in *Proceedings, 19th Real Time Conference (RT2014): Nara, Japan, May 26-30, 2014* (2014).

[60] *Petiroc-2a*, https://www.weeroc.com/en/products/petiroc-2a.

[61] K. Emi et al., Nucl. Instrum. Meth. **A379**, 225 (1996).

[62] I. Skorodumina et al., *CLAS12 Note 2017-001*, https://arxiv.org/abs/1703.08081,https://github.com/JeffersonLab/Hybrid-Baryons.

[63] M. Amarian et al., *JLab PR12-06-113*, https://www.jlab.org/exp_prog/proposals/06/PR12-06-113.pdf.

[64] H. C. Fenker et al., Nucl. Instrum. Meth. **A592**, 273 (2008).

[65] F. Sauli, Nucl. Instrum. Meth. **A386**, 531 (1997).